

Article

Simultaneous Removal of Nitrate and Phosphate in a Pyrrhotite and Sulfur-Circulating Packed Bed Reactor

Meiling Yu ^{1,2}, Yongyou Hu ^{1,2,*}, Donghui Liang ^{1,3,*}, Guobin Wang ⁴, Xiaoqiang Zhu ^{1,4} and Jieyun Xie ⁴

¹ School of Environment and Energy, South China University of Technology, Guangzhou Higher Education Mega Centre, Guangzhou 510006, China

² The Key Lab of Pollution Control and Ecosystem Restoration in Industry Clusters, Ministry of Education, South China University of Technology, Guangzhou Higher Education Mega Centre, Guangzhou 510006, China

³ College of Urban and Rural Construction, Zhongkai University of Agriculture and Engineering, Zhongkai Road, Haizhu District, Guangzhou 510225, China

⁴ Pengkai Environment Technology Co., Ltd., Guangzhou 511493, China

* Correspondence: ppyyhu@scut.edu.cn (Y.H.); liangdonghui0303@163.com (D.L.); Tel.: +86-136-0274-6125 (Y.H.); +86-187-2935-8153 (D.L.)

Abstract: A pyrrhotite and sulfur-circulating packed bed reactor (PS-CPBR) was constructed to study the removal process and mechanism of NO_3^- -N and PO_4^{3-} -P with different electron donors. The results showed that the NO_3^- -N and PO_4^{3-} -P removal performance of mixed electron donors (pyrrhotite and sulfur) was superior to the single electron donor (pyrrhotite). The optimum conditions of NO_3^- -N and PO_4^{3-} -P removal in the PS-CPBR were a hydraulic retention time (HRT) of 12 h and a C/N of 0, and the average removal efficiency was 100% and 86.39%. The sulfur in mixed electron donors was able to promote the dissolution of pyrrhotite and the formation of polysulfide to increase the effectiveness of electron donors, promoting the removal of NO_3^- -N, while the PO_4^{3-} -P was removed in the form of FePO_4 precipitation. Microbial and functional gene analyses demonstrated that different electron donors were able to influence the abundance of microbial communities and denitrification functional genes. Meanwhile, mixed electron donors were able to increase the protein content of biofilms and reduce the resistance of electron transfer between microorganisms and electrons.

Keywords: pyrrhotite; sulfur; circulating packed bed reactor; nitrate; phosphate



Citation: Yu, M.; Hu, Y.; Liang, D.; Wang, G.; Zhu, X.; Xie, J. Simultaneous Removal of Nitrate and Phosphate in a Pyrrhotite and Sulfur-Circulating Packed Bed Reactor. *Water* **2023**, *15*, 2158. <https://doi.org/10.3390/w15122158>

Academic Editors: Saurabh Mishra, Abhijit Maiti and Jagdeep Kumar Nayak

Received: 5 April 2023

Revised: 1 June 2023

Accepted: 2 June 2023

Published: 7 June 2023



Copyright: © 2023 by the authors. Licensee MDPI, Basel, Switzerland. This article is an open access article distributed under the terms and conditions of the Creative Commons Attribution (CC BY) license (<https://creativecommons.org/licenses/by/4.0/>).

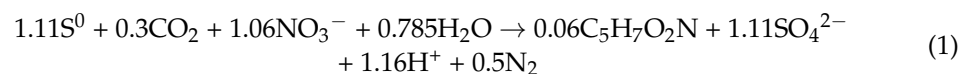
1. Introduction

Due to the widespread public concern about water environment protection and personal health issues, higher requirements have been placed on the discharge of nitrogen (N) and phosphorus (P) from wastewater treatment plants (WWTPs) [1,2]. It is necessary to add additional organic carbon sources or inorganic electron donors for biological denitrification. To meet higher P discharge standards, WWTPs need to use additional chemical reagents because their N and P removal efficiency is low, and the cost of the existing technology is high. Therefore, the development of efficient and economical technology to achieve dual control of N and P is the key to the discharge of nutrients in WWTPs.

Sulfur autotrophic denitrification (SAD) is regarded as an advanced technology for denitrification due to its advantages of having no additional organic carbon sources, a low sludge yield, and low operating costs [3–5]. Elemental sulfur is non-toxic, chemically stable, and the most commonly used electron for sulfur-based denitrification (Equation (1)). However, its low solubility (5 $\mu\text{g/L}$ at 25 °C) leads to an insufficient electron supply and a low N removal rate (<1000 $\text{g}\cdot\text{N}/\text{m}^3\cdot\text{d}$) [6], so its practical application in N removal in WWTPs is limited. When sulfur is used in the reactor, limestone is frequently used as a source of inorganic carbon and as a buffering agent to achieve N and P removal, but the

slow dissolution of limestone results in an insufficient alkalinity supply and a high effluent hardness in the system [7]. Therefore, more and more scholars have chosen to add NaHCO_3 to maintain alkalinity and improve water quality [8,9], but this change is not conducive to P removal. More effective measures are needed to achieve the goal of simultaneous N and P removal.

Pyrrhotite, which is easy to obtain and low in cost, is the main source of sulfur and iron in nature. It can be used as an electron for pyrrhotite autotrophic denitrification (PAD) (Equation (2)), formation of FePO_4 precipitation (Equation (3)), and adsorption of PO_4^{3-} -P (Equation (4)) to achieve N and P removal simultaneously [4,10,11]. In a range of aquatic environments, up to a third of NO_3^- -N removal is due to the PAD process [12]. However, the poor solubility of pyrrhotite makes the release of electron donors and iron ions unstable, so the efficiency of N and P removal is low. It limits the practical application of this technology in WWTPs that require rapid N and P removal. Thus, some scholars have improved the simultaneous N and P removal efficiency of the system by reducing the particle size and using mixed electron donors. Reducing the particle size increases the specific surface area (SSA) of pyrrhotite and enhances the contact of microorganisms with electron donors. For example, the scholars of [11] developed SSA (250–425 μm) nano pyrrhotite NPyr to achieve a high N removal rate (165 $\text{g}\cdot\text{N}/\text{m}^3\cdot\text{d}$), and the effluent was able to meet strict N and P discharge standards. However, the complex operation of making nanomaterials also increases the cost of use. Mixed electron donors can compensate for the lack of the single electron donor. The scholars of [13] used sulfur, pyrite, and fixed organic carbon sources to construct a reactor, which increased the electron donor supply and iron ion content and improved the stability of the reactor. The N and P removal efficiency was over 90% and 83%, respectively. This method is easy to implement and has more application value and economic benefits.



To further improve the electron donor and iron ion supply capacities of the system, some scholars have improved the efficiency of simultaneous N and P removal through reactor design. A pyrrhotite-limestone autotrophic denitrification biofilter (PADB) was constructed under the condition of the HRT of 12 h, and the removal efficiency of NO_3^- -N and PO_4^{3-} -P was 21.12% and 42.79% (the influent TON (NO_3^- -N + NO_2^- -N) and PO_4^{3-} -P were about 26.70 and 6.10 mg/L) [10]. This can be compared with the scholars of [4], who constructed pyrrhotite-sulfur-limestone autotrophic denitrification (PSLAD). When the HRT was 3 h, the NO_3^- -N and PO_4^{3-} -P removal efficiency was 98.44% and 100% (the influent TON and PO_4^{3-} -P were about 18.00 and 0.50 mg/L). Through comparison, it is not difficult to find that after the addition of sulfur, the removal efficiency of NO_3^- -N was significantly increased, and the HRT was greatly reduced. This is because the SAD process generates H^+ , promotes the dissolution of pyrrhotite (Equation (1)), improves the defect of an insufficient electron supply of pyrrhotite, and provides more available electron donors for microorganisms. Some scholars have adopted the circular operation method to improve the mass transfer rate of the reactor [3,8,14]. Some scholars have also adopted the layered filling method to reduce the packing compaction and maintain the high efficiency of N and P removal [7,15]. However, little information is available on sulfur and pyrrhotite as mixed electron donors to construct the reactor for NO_3^- -N and PO_4^{3-} -P removal simultaneously.

The main objectives of this work were: (1) construct a pyrrhotite and sulfur-circulating packed bed reactor (PS-CPBR) and explore the ability and efficiency of the PS-CPBR for NO_3^- -N and PO_4^{3-} -P removal; (2) evaluate the removal capability of NO_3^- -N and PO_4^{3-} -P under different HRT and C/N ratios in the PS-CPBR; (3) clarify the electron transfer mechanism and denitrification mechanism via electrochemical, microbial community structures, and denitrification functional gene analysis; (4) elucidate the PO_4^{3-} -P removal mechanism by SEM and XPS analysis. This work provides a basis for the removal of NO_3^- -N and PO_4^{3-} -P by the PS-CPBR.

2. Materials and Methods

2.1. Materials

2.1.1. Pyrrhotite and Sulfur

Pyrrhotite and sulfur were obtained from the Inner Mongolia Autonomous Region and Chengdu, Sichuan Province, respectively, in China. Pyrrhotite and sulfur were sieved into 3–5 mm particles and then stored in sealed plastic bags filled with N_2 to prevent oxidation. As analyzed by the X-ray diffractometer (Empyrean, PANalytical, Almelo, The Netherlands), the pyrrhotite was composed of the pyrrhotite mineral phase (Figure S1). The sulfur was of analytical grade with a purity $\geq 99.99\%$.

2.1.2. Inoculation Sludge and Culture Medium

Anaerobic sludge (AS) was taken from a WWTP in Guangzhou, Guangdong Province, China. A total of 20% (*v/v*) of the AS was seeded into the reactors to enrich the sulfur autotrophic denitrifying bacteria. The composition of the medium was consistent with the literature [10]. During the acclimatization period, the medium was replaced every 7 days, and the NO_3^- -N concentration changes were measured each cycle. The acclimatization and enrichment of sulfur autotrophic denitrifying bacteria were completed with a NO_3^- -N removal efficiency of 90%. Residual NO_3^- -N and SO_4^{2-} were removed before inoculation using the method in the literature [16].

2.1.3. Synthetic Wastewater

The components of the synthetic wastewater (SW) were shown in Table 1. KNO_3 , KH_2PO_4 , and NaHCO_3 were used as the nitrogen source, phosphorus source, and alkalinity, respectively. The influent NO_3^- -N and PO_4^{3-} -P concentrations were 30 and 3 mg/L. In phases I–V, 800 mg/L NaHCO_3 was added to the influent and reduced to 400 mg/L in phase VI. In phases IV–VI, sodium acetate was used as the organic carbon source, and the C/N (W/W) ratios were 1.0, 2.0, and 2.4, respectively. The trace element solution concentration was 2 mL/L. The initial pH of the influent was adjusted to 7.00 ± 0.20 with 1 mol/L HCl and 1 mol/L NaOH. The prepared fresh synthetic wastewater was deoxygenated with N_2 for 30 min.

Table 1. Synthetic wastewater.

Phases	I	II	III	IV	V	VI
Days	1–14	15–28	29–42	43–56	57–70	71–84
HRT	12	8	4	4	4	4
NO_3^- -N (mg/L)	30	30	30	30	30	30
PO_4^{3-} -P (mg/L)	3	3	3	3	3	3
Influent alkalinity (mg/L CaCO_3)	476	476	476	476	476	238
COD (provided by sodium acetate) / NO_3^- -N	–	–	–	1.0	2.0	2.4

2.1.4. Reactor Setup

Two parallel circulating packed bed reactors were constructed with an internal diameter of 7 cm, an effective height of 48 cm, and an effective volume of 1.7 L. The PS-CPBR fillers were pyrrhotite and sulfur (the volume ratio of pyrrhotite and sulfur was 3: 2), and

the P-CPBR filler was pyrrhotite. The filling ratio was 45%, and it was filled in three layers; the height of each layer was 12 cm with an operating volume of 2 L. The external circulation system consisted of a water tank with a peristaltic pump (Figure 1), and the circulation flow rate was 320 mL/min.

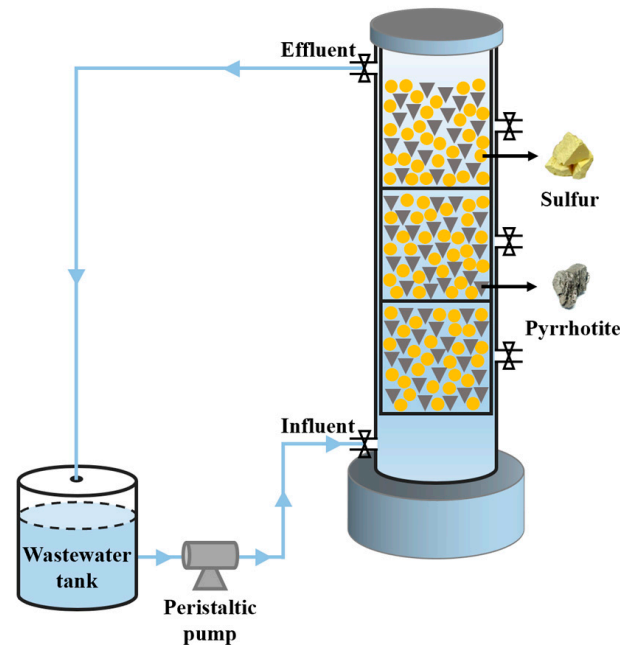


Figure 1. Configuration of pyrrhotite and sulfur-circulating packed bed reactor.

2.2. Methods

2.2.1. Reactor Start-Up and Operation Method

A total of 170 mL of acclimated AS was inoculated into the reactors, and the biofilm was attached to the carriers after 20 days (HRT was 24 h). In the operation phase, each reactor ran six phases of experiments. During the first three phases (I-III), the C/N was kept at 0 and the HRT was decreased from 12 h (phase I) to 4 h (phase III), exploring the influence of HRT on the removal of NO_3^- -N and PO_4^{3-} -P. In phases IV-VI, the HRT was kept at 4 h, and the C/N ratio was increased from 1.0 (phase IV) to 2.4 (phase VI), exploring the influence of the C/N ratio on the removal of NO_3^- -N and PO_4^{3-} -P. Each phase was tested for 14 days. The concentrations of NO_3^- -N, NO_2^- -N, TN, PO_4^{3-} -P, SO_4^{2-} , pH, and alkalinity were measured each cycle during the 84 days of continuous operation. All the samples were filtered through a 0.45 μm filter before measuring.

2.2.2. Conventional Index Determination Method

All detection methods referred to the Standard Methods [17].

2.2.3. Precipitation Substance Analysis Method

The filler samples were randomly collected from each reactor at phase VI to obtain the precipitation substance on each filler surface. The morphology of the precipitation substance was determined using scanning electron microscopy (Merlin, Zeiss, Oberkochen, Germany). The phase composition and atomic valence state of the precipitation substances were analyzed using X-ray photoelectron spectroscopy (Escalab Xi+, ThermoFisher, Oxford, UK).

2.2.4. Analyses of Biofilm

Extracellular polymeric substances (EPS) affect the cell surface charge, hydrophilicity, and hydrophobicity, and have certain effects on the metabolic activity of cells [18]. The biofilm samples were randomly collected from each reactor during phase III, and

the ultrasonic–thermal extraction method of EPS in the biofilm was referred to [19]. The concentrations of protein (PN) and polysaccharide (PS) in the EPS were determined using the Bradford method and the phenol–sulfuric acid method [20,21]. Cyclic voltammetry (CV) was able to identify the redox reaction between microorganisms and electron donors. Electrochemical impedance spectroscopy (EIS) was able to determine the system’s internal resistance, which indicated the speed of electron transfer. The CV and EIS between the pyrrhotite, sulfur, and microorganisms were determined using an electrochemical workstation (CHI 660D, CH Instrument Company, Beijing, China) [22].

2.2.5. The Detection Methods of Community Structure and Functional Gene

The evolutions of microbial community structures in the two reactors were analyzed through high-throughput amplicon sequencing. Biofilm samples were collected from the PS-CPBR and the P-CPBR at the start-up phase (CK1–CK2), and phase VI (VI1–VI2). The amplified products were purified and sequenced by Shanghai Passino Biotechnology Co., Ltd., using the Illumina MiSeq high-throughput sequencer (Illumina, San Diego, CA, USA). The MiSeq data were classified and analyzed on the Genescloud platform. Biofilm samples were randomly collected from the two reactors after the end of phase VI, and the abundance of functional genes related to denitrification (NapA, NarG, NirK, NirS, NorB, Nor, and NosZ) were analyzed using the absolute quantitative PCR (AQ-PCR) technique.

2.2.6. Data Processing Method

The calculation method of the pollutant removal efficiency is introduced in detail in the Text S1.

3. Results

3.1. Performance of the PS-CPBR

3.1.1. The Removal Efficiency of NO_3^- -N and PO_4^{3-} -P

The effects of HRT (phases I–III) and C/N (phases IV–VI) on the NO_3^- -N and PO_4^{3-} -P removal efficiency in the two reactors (PS-CPBR and P-CPBR) were shown in Figure 2a,b, and concentration changes in NO_3^- -N and PO_4^{3-} -P were shown in Figure 2c,d. In phases I–III, the C/N was kept at 0, and the HRT was decreased from 12 h (phase I) to 4 h (phase III). With the decrease in HRT (from 12 h to 4 h), the removal efficiency of NO_3^- -N and PO_4^{3-} -P showed a decreasing trend in the two reactors. This result was possibly due to the insoluble character of the solid electron donor, the short HRT resulted in less dissolution of electron donors and iron ions and further reduced the removal efficiency of NO_3^- -N and PO_4^{3-} -P. It was consistent with the research result that prolonging HRT is more conducive to NO_3^- -N and PO_4^{3-} -P removal [23]. When the HRT decreased to 4 h (phase III), the removal efficiency of NO_3^- -N and PO_4^{3-} -P was maintained at 67.47% and 45.81% in the PS-CPBR, but only 18.13% and 14.89% in the P-CPBR. This might be because the SAD process produced H^+ , which promoted the dissolution of pyrrhotite and increased the supply of electron donors and iron ions in the PS-CPBR. The NO_3^- -N and PO_4^{3-} -P removal efficiency of this research was superior to previous research [10]. In phases IV–VI, the HRT was kept at 4 h, and the C/N ratio was decreased from 1.0 (phase IV) to 2.4 (phase VI). The NO_3^- -N removal efficiency in the two reactors increased. NO_3^- -N was able to be removed completely when the C/N ratio was 2.0 in the PS-CPBR, while the C/N ratio needed to be adjusted to 2.4 in the P-CPBR to achieve the same NO_3^- -N removal effect. This result further proved that the PS-CPBR provided richer electron donors than the P-CPBR and achieved higher NO_3^- -N removal performance. Although the PO_4^{3-} -P removal efficiency in the P-CPBR was higher than the PS-CPBR, the PO_4^{3-} -P removal efficiency in the two reactors was under a downward trend with the increased ratio of C/N. The result might be caused by the increase in the carbon source promoting the growth of bacteria, and a large number of microorganisms were attached to the surface of the pyrrhotite, hindering the release of iron ions. Meanwhile, the presence of sulfur in the PS-CPBR promoted the dissolution of pyrrhotite and increased the concentration of soluble

iron ions. Thus, it improved the removal efficiency of $\text{PO}_4^{3-}\text{-P}$. Under the condition of HRT of 12 h and C/N of 0 (phase I), the average removal efficiency of $\text{NO}_3^- \text{-N}$ and $\text{PO}_4^{3-}\text{-P}$ was 100.00% and 86.39%. This showed that prolonging the HRT was more beneficial to the PS-CPBR to maintain the efficient removal of $\text{NO}_3^- \text{-N}$ and $\text{PO}_4^{3-}\text{-P}$. Through the above comparison, it was not difficult to find that the removal effects of $\text{NO}_3^- \text{-N}$ and $\text{PO}_4^{3-}\text{-P}$ by the pyrrhotite and sulfur as mixed electron donors (PS-CPBR) was better than the single pyrrhotite electron donor (P-CPBR).

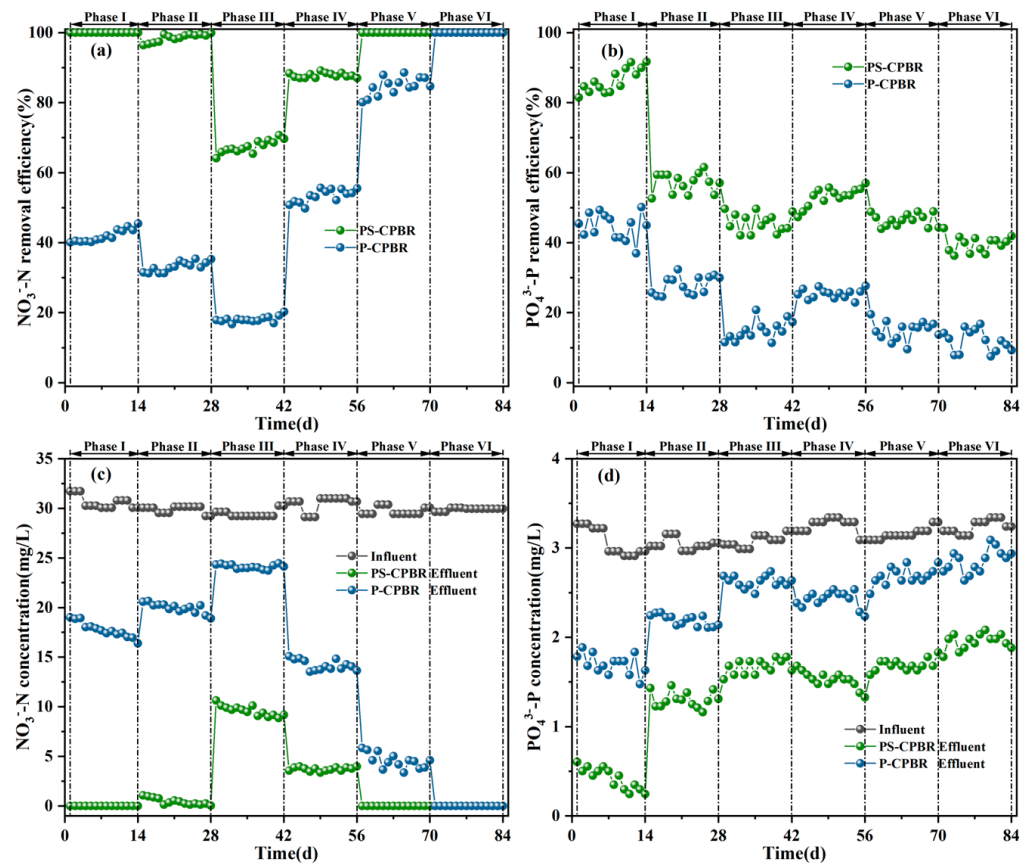


Figure 2. Nitrogen and phosphorus removal performance of the PS-CPBR and the P-CPBR during the operation phases: (a) $\text{NO}_3^- \text{-N}$ removal efficiency, (b) $\text{PO}_4^{3-}\text{-P}$ removal efficiency, (c) $\text{NO}_3^- \text{-N}$ concentration, and (d) $\text{PO}_4^{3-}\text{-P}$ concentration.

The TN concentration changes were shown in Figure 3a. It could be seen that the TN removal performance in the PS-CPBR was better than the P-CPBR. The TN removal efficiency was under a downward trend, which was consistent with the trend of $\text{NO}_3^- \text{-N}$ (phases I-VI). The difference in TN removal efficiency between the two reactors was mainly reflected in the $\text{NO}_2^- \text{-N}$ accumulation. Except for phases II-III, the $\text{NO}_2^- \text{-N}$ concentration in the PS-CPBR was lower than that in the P-CPBR in other phases (Figure 3b). In phase I, the TN removal efficiency of the PS-CPBR was 2.93 times higher than the P-CPBR, while the $\text{NO}_2^- \text{-N}$ concentration in the PS-CPBR was only 36.7% of that in the P-CPBR. In phase V, the TN removal efficiency of the PS-CPBR was 1.33 times higher than the P-CPBR. At this time, there was no $\text{NO}_2^- \text{-N}$ accumulation in the PS-CPBR, while 2.54 mg/L $\text{NO}_2^- \text{-N}$ was accumulated in the P-CPBR. This indicated that the PS-CPBR system had a lower $\text{NO}_2^- \text{-N}$ accumulation and a higher TN removal efficiency. This might be because the mixed electron donors provided more effective electron donors, which were able to reduce the accumulation of $\text{NO}_2^- \text{-N}$ and increase the removal efficiency of TN.

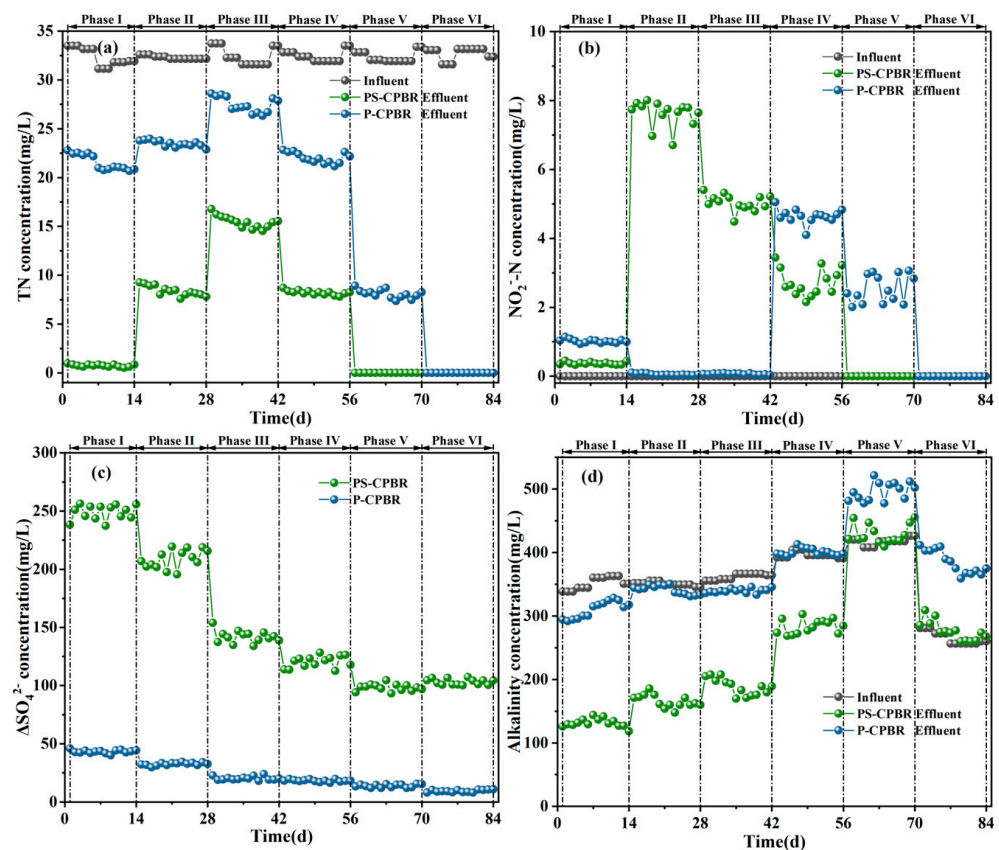


Figure 3. The variations in concentrations in the PS-CPBR and the P-CPBR during the operation phases: (a) TN, (b) NO_2^- -N, (c) ΔSO_4^{2-} —difference between effluent and influent SO_4^{2-} , and (d) alkalinity (as CaCO_3).

3.1.2. Sulfate Generation and Alkalinity Consumption

As shown in Figure 3c, SO_4^{2-} was produced in the PS-CPBR and the P-CPBR during the denitrification process. When single sulfur and pyrrhotite were used as electron donors to remove NO_3^- -N, the theoretical yield of SO_4^{2-} was $7.54 \text{ mg SO}_4^{2-} / \text{mg NO}_3^-$ -N and $3.80 \text{ mg SO}_4^{2-} / \text{mg NO}_3^-$ -N, respectively (Equations (1) and (2)). During the whole operation phase, the effluent concentrations of SO_4^{2-} in the PS-CPBR and the P-CPBR gradually decreased (phases I–VI), and the effluent concentration of SO_4^{2-} in the PS-CPBR was higher than in the P-CPBR. This might be because the mixed electron donors were able to increase the supply of electron donors and promote the autotrophic denitrification process, so the SO_4^{2-} yield was higher than the single electron donor. The yield of SO_4^{2-} in the PS-CPBR was lower than the theoretical value, this situation might be because shortening the HRT led to incomplete denitrification. Meanwhile, the addition of the organic carbon source promoted the growth of heterotrophic microorganisms, and the microorganisms used organic matter for denitrification rather than inorganic electron donors (pyrrhotite and sulfur). Overall, mixotrophic denitrification was able to significantly improve denitrification efficiency and reduce SO_4^{2-} concentration in the effluent.

The changes in alkalinity in the two reactors were shown in Figure 3d. During all of the operation phase, the alkalinity consumption in the P-CPBR was lower than that in the PS-CPBR. This might be because the SAD process produced a large amount of H^+ , which consumed more alkalinity ($4.57 \text{ g CaCO}_3 / \text{g NO}_3^-$ -N). After the addition of organic carbon sources (phases V–VI), the consumption of alkalinity in the PS-CPBR was reduced significantly, indicating that no additional alkalinity supplement was needed when the C/N ratio was greater than 2.0. Overall, adding an appropriate amount of organic carbon source to the PS-CPBR was able to improve NO_3^- -N removal efficiency and reduce the consumption of alkalinity [24].

3.2. Mechanism of NO_3^- -N Removal

3.2.1. Electron Transfer Mechanism

Figure 4a showed the variation in the EPS content in the two reactors. The total content of EPS in the PS-CPBR was higher than that in the P-CPBR, indicating that the microorganisms in the PS-CPBR had better tolerance to external environmental changes [25]. The increase in PN in the EPS was able to promote the stability and aggregation of the biofilm structure [18]. The content of PN in the PS-CPBR was higher than that in the P-CPBR, which indicated that the biofilm structure was more stable to maintain the stability of the PS-CPBR during the operation phase. Overall, the variation in the EPS was mainly attributed to the difference in electron donors. Mixed electron donors were more conducive to the microorganisms generating more EPS and improved the stability and electron transfer rate of the system. Meanwhile, the system improved its adaptability to adverse environments.

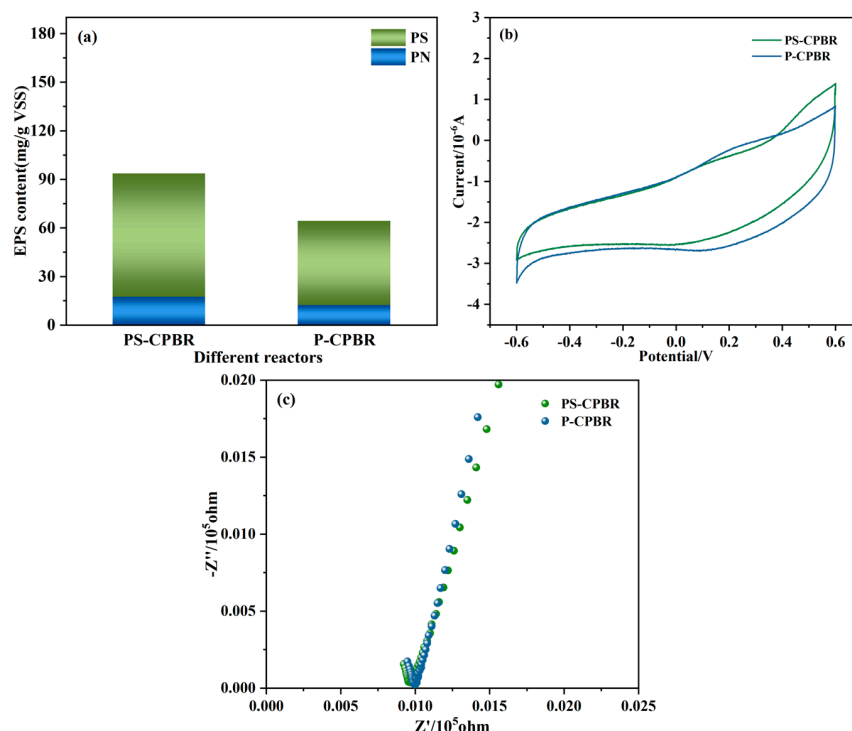


Figure 4. Electron transfer in the PS-CPBR and the P-CPBR: (a) concentration change of EPS, (b) electrochemical characterization curve of CV, and (c) electrochemical characterization curve of EIS.

The CV curve showed that reduction and oxidation peaks appeared in the two reactors (Figure 4b). The intensity of the redox peaks reflected the magnitude of the current intensity [26], so it could be concluded that the current intensity in the PS-CPBR was greater than that in the P-CPBR. Compared to the EIS curve in Figure 4c, it could be concluded that the charge transfer resistance in the PS-CPBR was smaller than that in the P-CPBR. The scholars of [27] concluded that reducing the resistance was able to speed up the electron transfer rate, which meant that the electron transfer rate in the PS-CPBR was higher than that in the P-CPBR. This was consistent with Section 3.1.1 in that the PS-CPBR performed higher NO_3^- -N efficiency than the P-CPBR. Combined with the EPS and electrochemical analysis results, it could be concluded that the mixed electron donors (pyrrhotite and sulfur) promoted the generation of more PN by the microorganisms to promote the electron transfer between microorganisms and electrons and promoted the electron transfer rate by reducing the resistance.

3.2.2. Evolution of Microbial Community Structures and Functional Bacteria

Biofilms were collected from the two reactors at the start-up and the final phase. To compare differences in microbial communities with different electron donors, the changes

in microbial community structures were analyzed at the phylum and genus levels. In the microbial community structure at the phylum level, there was not a significant difference between CK1, CK2, VI1, and VI2 (Figure 5a). The main phyla in the four samples were *Proteobacteria* and *Bacteroidetes*, and these phyla widely existed in various wastewater treatment processes. *Proteobacteria* played a dominant role in biological anoxic and anaerobic denitrification [28,29]. *Bacteroidetes* mainly participated in biological anoxic denitrification [30]. Meanwhile, the abundance of the dominant phylum in the PS-CPBR was relatively stable, and these results indicated that the mixed electron donors in the PS-CPBR acted as a carrier to support the growth of biofilm, which was more conducive to the retention of biomass. The genus level distributions of the microbial communities were shown in Figure 5b. *Thiobacillus* was the dominant genus in CK1 and CK2. *Thiobacillus* was a facultative anaerobic and obligate chemoautotrophic sulfur-oxidizing bacterium. The high abundance of *Thiobacillus* was consistent with previous studies in sulfur-based bioreactors [31–33]. *Thiobacillus* had a strong NAFO ability and oxidized minerals function under anaerobic conditions, which was able to promote denitrification efficiency [34]. The dominant bacterial genera in the two reactors changed greatly in VI1 and VI2. The dominant bacterial genera in the PS-CPBR (VI1) were *Dechloromonas* (25.93%), *Thiomonas* (12.99%), and *Geobacter* (13.66%). The main dominant genera in the P-CPBR (VI2) were *Zoogloea* (37.77%), *Alicyclophilus* (7.81%), and *Thauera* (6.06%). These results demonstrated that the diversity of the microbial communities in the PS-CPBR was significantly higher than that in the P-CPBR. New dominant bacteria appeared through adding organic carbon to the reactors. Among them, *Dechloromonas* was able to oxidize Fe^{2+} to Fe^{3+} and provided electrons for denitrification. *Geobacter* was able to reduce sulfur to sulfide [35], which played a crucial role in sulfide generation and the denitrification process in the PS-CPBR system. The above results indicated that the composition of the electron donors lead to a large difference in the diversity of the microbial communities.

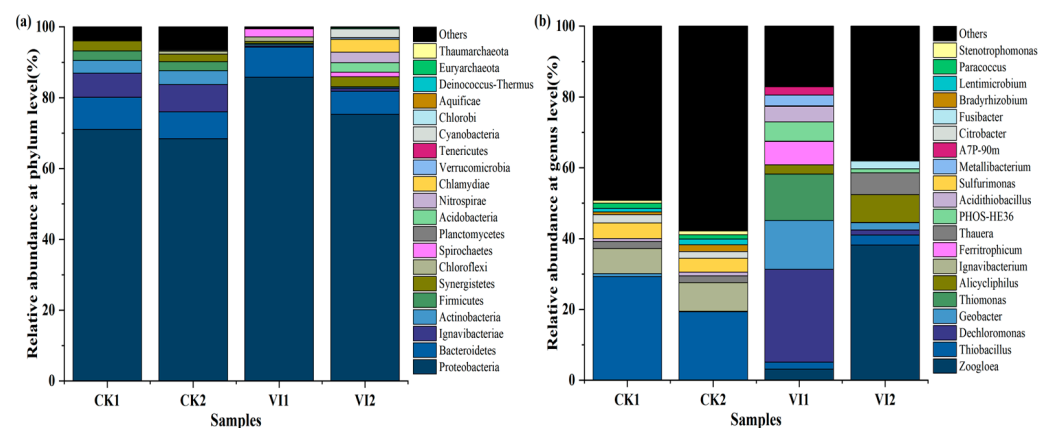


Figure 5. Classification of 16s rRNA gene sequences of microbial communities on the filter biofilms in the PS-CPBR and the P-CPBR: (a) phylum level and (b) genus level (relative abundance $\geq 1\%$).

3.2.3. Denitrification Functional Genes and Denitrification Pathways

The absolute abundance of functional genes related to denitrification was determined by the AQ-PCR technique (as shown in Table S1). The results showed that both reactors contained functional genes related to denitrification (NapA/NarG, NirK/NirS, NorB/Nor, and NosZ). The NarG gene was mainly expressed in anaerobic conditions, while the NapA gene was mainly expressed in hypoxic conditions [36]. The NarG gene abundance in the two reactors was significantly higher than the NapA gene because the reactor was placed in an anaerobic environment after the deoxygenation of the influent. The NirS/NirK genes were a group of key coding genes that catalyzed reductive NO_2^- -N to NO [37]. The NirS gene abundance in the PS-CPBR was up to 8.21×10^6 copy/g, which realized the process of reducing NO_2^- -N to NO. The abundance of the NO reductase NosZ was higher than the NO reductase NorB/Nor, indicating that the N_2O could be quickly reduced to N_2 , and

there was no N_2O accumulation during denitrification. Therefore, the application of the PS-CPBR for N removal was able to control the emission of the greenhouse gas N_2O [38]. In this study, the two reactors contained genes that encoded enzymes involved in converting NO_3^- -N into N_2 . However, the abundance of genes related to the NO_3^- -N reduction in the PS-CPBR was higher than that in the P-CPBR (NapA/NarG, NirK/NirS, NorB, and NosZ) (Table S1). It was consistent with the results (Section 3.1.1) that the PS-CPBR achieved a higher NO_3^- -N removal efficiency.

The autotrophic denitrifying bacteria were able to use a variety of reducible sulfur and iron sulfides as electron donors for denitrification. Polysulfide was formed from the abiotic reaction between sulfur and sulfide under neutral or alkaline conditions [8]. The presence of polysulfide increased the sulfur bioavailability and N removal efficiency [14,39]. The XPS spectrum of S (Figure 6) revealed a dominant peak of the S 2p spectrum at 163.5 eV, which was identified as S_n^{2-} 2p_{3/2} [8,14,40]. This might be because the HS^- generated by pyrrhotite dissolution under anaerobic conditions [41] reacted with sulfur to form a polysulfide (Equation (5)), which was more effective than pyrrhotite and sulfur. So, it was more suitable as an electron donor for the denitrification process (Equation (6)) [8]. The production of polysulfide might be one of the important reasons why the performance of the PS-CPBR in removing NO_3^- -N was better than the P-CPBR. At the same time, the SAD process produced H^+ to promote the dissolution of pyrrhotite, so the PS-CPBR system was able to provide microorganisms with a variety of electron donors (HS^- , S^0 , S_n^{2-}). It was also able to extend the reaction zone from the solid surface to the liquid phase, which improved the effectiveness of solid electrons significantly [33]. Finally, the effective removal of NO_3^- -N was achieved.

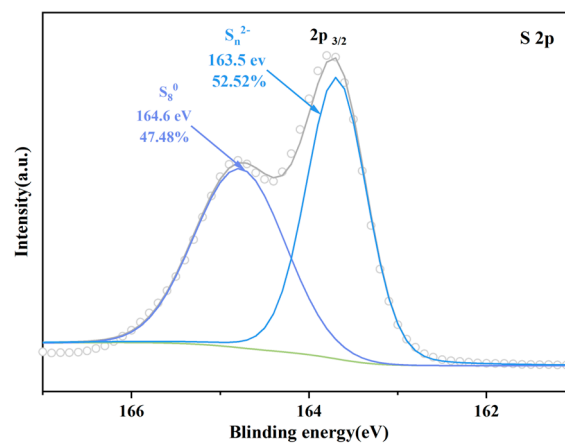
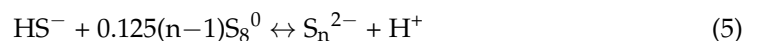


Figure 6. XPS spectrum of S 2p of PS-CPBR.

3.3. PO_4^{3-} -P Removal Mechanism

The two reactors operated in an anaerobic environment, and phosphorus-accumulating bacteria were not detected in the reactors (Section 3.2.2), indicating that biological phosphorus removal did not play a dominant role in the PO_4^{3-} -P removal process. The precipitation substances in the PS-CPBR were secondary minerals and formed spherical crystals (Figure 7a). The XPS spectrum of Fe (Figure 7b) showed that a dominant peak of the Fe 2p spectrum, located at 707.4 eV, corresponded to FeS_2 2p_{3/2} [42]. Two other peaks, at 710.6 eV and 713.5 eV, were identified as Fe^{3+} 2p_{3/2} [43,44]. There was also a peak at 724.0 eV, which was identified as Fe^{2+} 2p_{1/2} [44]. Fe^{3+} and Fe^{2+} were detected simultaneously in the sediment, and the solubility product constant (K_{sp}) of ferrous phosphate was much lower than that of ferric phosphate. The mechanisms of the PO_4^{3-} -P removal in the PS-CPBR were as

follows: First, there was the dissolution of pyrrhotite to release soluble Fe^{2+} , and part of the Fe^{2+} combined with PO_4^{3-} -P to form $\text{Fe}_3(\text{PO}_4)_2$. Secondly, the $\text{Fe}_3(\text{PO}_4)_2$ precipitation was able to be further oxidized by *Dechloromonas* and *Ferritrophicum* to form FePO_4 [45,46]. This study confirmed that PO_4^{3-} -P was removed in the form of FePO_4 precipitation. The above results were consistent with the other researchs [4,10].

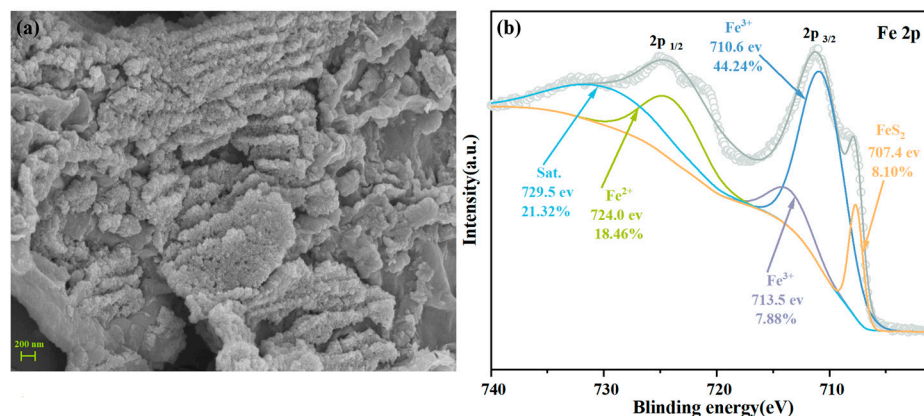


Figure 7. Precipitation substances in the PS-CPBR: (a) SEM image (scale bar: 200 nm), (b) XPS spectrum of Fe 2p.

4. Conclusions

This study showed that the PS-CPBR was able to remove NO_3^- -N and PO_4^{3-} -P. When the HRT was 12 h and the C/N was 0, the average removal efficiency of NO_3^- -N and PO_4^{3-} -P was 100% and 86.39%. Sulfur promoted the dissolution of pyrrhotite and the formation of polysulfide, which increased the effectiveness of the electrons. Mixed electrons were able to increase the diversity of the microbial communities and the abundance of denitrification functional genes. Meanwhile, mixed electrons were able to increase the PN and reduce the resistance to accelerating the electron transfer rate. PO_4^{3-} -P was removed by forming FePO_4 . The next phase should focus on increasing the effectiveness of pyrrhotite and sulfur.

Supplementary Materials: The following supporting information can be downloaded at: <https://www.mdpi.com/article/10.3390/w15122158/s1>, Text S1: Data processing method; Figure S1: XRD pattern of pyrrhotite; Table S1: Absolute abundance of denitrification genes in the two reactors.

Author Contributions: Conceptualization, M.Y. and Y.H.; methodology, M.Y.; software, M.Y.; validation, M.Y. and D.L.; formal analysis, M.Y. and D.L.; investigation, M.Y.; resources, M.Y.; data curation, M.Y.; writing—original draft preparation, M.Y.; writing—review and editing, Y.H.; visualization, M.Y.; supervision, Y.H.; project administration, M.Y., Y.H. and D.L.; funding acquisition, G.W., X.Z. and J.X. All authors have read and agreed to the published version of the manuscript.

Funding: This research was funded by National Natural Science Foundation of China (No. 21477039) and Pengkai Environment Technology Co., Ltd.

Data Availability Statement: Not applicable.

Acknowledgments: The authors gratefully thank the financial support provided by National Natural Science Foundation of China (No. 21477039) and Pengkai Environment Technology Co., Ltd.

Conflicts of Interest: The authors declare no conflict of interest.

References

1. Kitsiou, D.; Karydis, M. Coastal marine eutrophication assessment: A review on data analysis. *Environ. Int.* **2011**, *37*, 778–801. [CrossRef] [PubMed]
2. Poikane, S.; Kelly, M.G.; Salas Herrero, F.; Pitt, J.A.; Jarvie, H.P.; Claussen, U.; Leujak, W.; Lyche Solheim, A.; Teixeira, H.; Phillips, G. Nutrient criteria for surface waters under the European Water Framework Directive: Current state-of-the-art, challenges and future outlook. *Sci. Total Environ.* **2019**, *695*, 133888. [CrossRef] [PubMed]

3. Di Capua, F.; Mascolo, M.C.; Pirozzi, F.; Esposito, G. Simultaneous denitrification, phosphorus recovery and low sulfate production in a recirculated pyrite-packed biofilter (RPPB). *Chemosphere* **2020**, *255*, 126977. [[CrossRef](#)] [[PubMed](#)]
4. Li, R.; Wei, D.; Wang, W.; Zhang, Y. Pyrrhotite-sulfur autotrophic denitrification for deep and efficient nitrate and phosphate removal: Synergistic effects, secondary minerals and microbial community shifts. *Bioresour. Technol.* **2020**, *308*, 123302. [[CrossRef](#)]
5. Zhou, Y.; Chen, F.; Chen, N.; Peng, T.; Dong, S.; Feng, C. Denitrification performance and mechanism of biofilter constructed with sulfur autotrophic denitrification composite filler in engineering application. *Bioresour. Technol.* **2021**, *340*, 125699. [[CrossRef](#)] [[PubMed](#)]
6. Di Capua, F.; Ahoranta, S.H.; Papirio, S.; Lens, P.N.L.; Esposito, G. Impacts of sulfur source and temperature on sulfur-driven denitrification by pure and mixed cultures of *Thiobacillus*. *Process Biochem.* **2016**, *51*, 1576–1584. [[CrossRef](#)]
7. Li, Y.; Wang, Y.; Wan, D.; Li, B.; Zhang, P.; Wang, H. Pilot-scale application of sulfur-limestone autotrophic denitrification biofilter for municipal tailwater treatment: Performance and microbial community structure. *Bioresour. Technol.* **2020**, *300*, 122682. [[CrossRef](#)]
8. Qiu, Y.Y.; Gong, X.; Zhang, L.; Zhou, S.; Li, G.; Jiang, F. Achieving a Novel Polysulfide-Involved Sulfur-Based Autotrophic Denitrification Process for High-Rate Nitrogen Removal in Elemental Sulfur-Packed Bed Reactors. *ACS EST Eng.* **2022**, *2*, 1504–1513. [[CrossRef](#)]
9. Sahinkaya, E.; Dursun, N. Use of elemental sulfur and thiosulfate as electron sources for water denitrification. *Bioprocess Biosyst. Eng.* **2015**, *38*, 531–541. [[CrossRef](#)]
10. Li, R.; Morrison, L.; Collins, G.; Li, A.; Zhan, X. Simultaneous nitrate and phosphate removal from wastewater lacking organic matter through microbial oxidation of pyrrhotite coupled to nitrate reduction. *Water Res.* **2016**, *96*, 32–41. [[CrossRef](#)]
11. Yang, Y.; Chen, T.; Morrison, L.; Gerrity, S.; Collins, G.; Porca, E.; Li, R.; Zhan, X. Nanostructured pyrrhotite supports autotrophic denitrification for simultaneous nitrogen and phosphorus removal from secondary effluents. *Chem. Eng. J.* **2017**, *328*, 511–518. [[CrossRef](#)]
12. Vaclavkova, S.; Jørgensen, C.J.; Jacobsen, O.S.; Aamand, J.; Elberling, B. The Importance of Microbial Iron Sulfide Oxidation for Nitrate Depletion in Anoxic Danish Sediments. *Aquat. Geochem.* **2014**, *20*, 419–435. [[CrossRef](#)]
13. Lu, X.; Wan, Y.; Zhong, Z.; Liu, B.; Zan, F.; Zhang, F.; Wu, X. Integrating sulfur, iron(II), and fixed organic carbon for mixotrophic denitrification in a composite filter bed reactor for decentralized wastewater treatment: Performance and microbial community. *Sci. Total Environ.* **2021**, *795*, 148825. [[CrossRef](#)] [[PubMed](#)]
14. Qiu, Y.Y.; Zhang, L.; Mu, X.; Li, G.; Guan, X.; Hong, J.; Jiang, F. Overlooked pathways of denitrification in a sulfur-based denitrification system with organic supplementation. *Water Res.* **2020**, *169*, 115084. [[CrossRef](#)]
15. Li, H.; Li, Y.; Guo, J.; Song, Y.; Hou, Y.; Lu, C.; Han, Y.; Shen, X.; Liu, B. Effect of calcinated pyrite on simultaneous ammonia, nitrate and phosphorus removal in the BAF system and the Fe(2+) regulatory mechanisms: Electron transfer and biofilm properties. *Environ. Res.* **2021**, *194*, 110708. [[CrossRef](#)]
16. Li, R.; Feng, C.; Hu, W.; Xi, B.; Chen, N.; Zhao, B.; Liu, Y.; Hao, C.; Pu, J. Woodchip-sulfur based heterotrophic and autotrophic denitrification (WSHAD) process for nitrate contaminated water remediation. *Water Res.* **2016**, *89*, 171–179. [[CrossRef](#)]
17. APHA. *Standard Methods for Water and Wastewater Examination*; American Public Health Association: Washington, DC, USA, 2005.
18. Shi, Y.; Huang, J.; Zeng, G.; Gu, Y.; Chen, Y.; Hu, Y.; Tang, B.; Zhou, J.; Yang, Y.; Shi, L. Exploiting extracellular polymeric substances (EPS) controlling strategies for performance enhancement of biological wastewater treatments: An overview. *Chemosphere* **2017**, *180*, 396–411. [[CrossRef](#)]
19. Hou, J.; You, G.X.; Xu, Y.; Wang, C.; Wang, P.F.; Miao, L.Z.; Li, Y.; Ao, Y.H.; Lv, B.W.; Yang, Y.Y. Long-term effects of CuO nanoparticles on the surface physicochemical properties of biofilms in a sequencing batch biofilm reactor. *Appl. Microbiol. Biotechnol.* **2016**, *100*, 9629–9639. [[CrossRef](#)]
20. Feng, X.; Wu, Q.; Che, L.; Ren, N. Analyzing the inhibitory effect of metabolic uncoupler on bacterial initial attachment and biofilm development and the underlying mechanism. *Environ. Res.* **2020**, *185*, 109390. [[CrossRef](#)]
21. Li, K.; Guo, J.; Li, H.; Han, Y.; Chen, Z.; Song, Y.; Xing, Y.; Zhang, C. A combined heterotrophic and sulfur-based autotrophic process to reduce high concentration perchlorate via anaerobic baffled reactors: Performance advantages of a step-feeding strategy. *Bioresour. Technol.* **2019**, *279*, 297–306. [[CrossRef](#)]
22. Fang, Y.; Deng, C.; Chen, J.; Lu, J.; Chen, S.; Zhou, S. Accelerating the start-up of the cathodic biofilm by adding acyl-homoserine lactone signaling molecules. *Bioresour. Technol.* **2018**, *266*, 548–554. [[CrossRef](#)] [[PubMed](#)]
23. Kong, Z.; Li, L.; Feng, C.; Dong, S.; Chen, N. Comparative investigation on integrated vertical-flow biofilters applying sulfur-based and pyrite-based autotrophic denitrification for domestic wastewater treatment. *Bioresour. Technol.* **2016**, *211*, 125–135. [[CrossRef](#)] [[PubMed](#)]
24. Tong, S.; Stocks, J.L.; Rodriguez-Gonzalez, L.C.; Feng, C.; Ergas, S.J. Effect of oyster shell medium and organic substrate on the performance of a particulate pyrite autotrophic denitrification (PPAD) process. *Bioresour. Technol.* **2017**, *244*, 296–303. [[CrossRef](#)] [[PubMed](#)]
25. Han, F.; Wei, D.; Ngo, H.H.; Guo, W.; Xu, W.; Du, B.; Wei, Q. Performance, microbial community and fluorescent characteristic of microbial products in a solid-phase denitrification biofilm reactor for WWTP effluent treatment. *J. Environ. Manag.* **2018**, *227*, 375–385. [[CrossRef](#)]
26. Kluepfel, L.; Keiluweit, M.; Kleber, M.; Sander, M. Redox Properties of Plant Biomass-Derived Black Carbon (Biochar). *Environ. Sci. Technol.* **2014**, *48*, 5601–5611. [[CrossRef](#)]

27. Zeng, C.P.; Li, Y.; Lu, A.H.; Ding, H.R.; Wang, X.; Wang, C.Q. Electrochemical Interaction of a Heterotrophic Bacteria *Alcaligenes faecalis* with a Graphite Cathode. *Geomicrobiol. J.* **2012**, *29*, 244–249. [[CrossRef](#)]
28. Li, L.; Dong, Y.; Qian, G.; Hu, X.; Ye, L. Performance and microbial community analysis of bio-electrocoagulation on simultaneous nitrification and denitrification in submerged membrane bioreactor at limited dissolved oxygen. *Bioresour. Technol.* **2018**, *258*, 168–176. [[CrossRef](#)]
29. Zhang, R.C.; Xu, X.J.; Chen, C.; Xing, D.F.; Shao, B.; Liu, W.Z.; Wang, A.J.; Lee, D.J.; Ren, N.Q. Interactions of functional bacteria and their contributions to the performance in integrated autotrophic and heterotrophic denitrification. *Water Res.* **2018**, *143*, 355–366. [[CrossRef](#)]
30. Yan, L.; Liu, S.; Liu, Q.; Zhang, M.; Liu, Y.; Wen, Y.; Chen, Z.; Zhang, Y.; Yang, Q. Improved performance of simultaneous nitrification and denitrification via nitrite in an oxygen-limited SBR by alternating the DO. *Bioresour. Technol.* **2019**, *275*, 153–162. [[CrossRef](#)]
31. Li, J. Long-Term Operation of a Pilot-Scale Sulfur-Based Autotrophic Denitrification System for Deep Nitrogen Removal. *Water* **2023**, *15*, 428.
32. Zhang, L.; Zhang, C.; Hu, C.; Liu, H.; Bai, Y.; Qu, J. Sulfur-based mixotrophic denitrification corresponding to different electron donors and microbial profiling in anoxic fluidized-bed membrane bioreactors. *Water Res.* **2015**, *85*, 422–431. [[CrossRef](#)] [[PubMed](#)]
33. Zhang, Q.; Wang, C.; Jiang, L.; Qi, J.; Wang, J.; He, X. Impact of dissolved oxygen on the microbial community structure of an intermittent biological aerated filter (IBAF) and the removal efficiency of gasification wastewater. *Bioresour. Technol.* **2018**, *255*, 198–204. [[CrossRef](#)] [[PubMed](#)]
34. Beller, H.R.; Chain, P.S.G.; Letain, T.E.; Chakicherla, A.; Larimer, F.W.; Richardson, P.M.; Coleman, M.A.; Wood, A.P.; Kelly, D.P. The genome sequence of the obligately chemolithoautotrophic, facultatively anaerobic bacterium *Thiobacillus denitrificans*. *J. Bacteriol.* **2006**, *188*, 1473–1488. [[CrossRef](#)] [[PubMed](#)]
35. Sun, R.; Zhang, L.; Zhang, Z.; Chen, G.H.; Jiang, F. Realizing high-rate sulfur reduction under sulfate-rich conditions in a biological sulfide production system to treat metal-laden wastewater deficient in organic matter. *Water Res.* **2018**, *131*, 239–245. [[CrossRef](#)]
36. Yang, J.; Feng, L.; Pi, S.; Cui, D.; Ma, F.; Zhao, H.P.; Li, A. A critical review of aerobic denitrification: Insights into the intracellular electron transfer. *Sci. Total Environ.* **2020**, *731*, 139080. [[CrossRef](#)]
37. Chen, Y.N.; Zhou, W.; Li, Y.P.; Zhang, J.C.; Zeng, G.M.; Huang, A.Z.; Huang, J.X. Nitrite reductase genes as functional markers to investigate diversity of denitrifying bacteria during agricultural waste composting. *Appl. Microbiol. Biotechnol.* **2014**, *98*, 4233–4243. [[CrossRef](#)]
38. Jia, L.; Sun, H.; Zhou, Q.; Dai, R.; Wu, W. Integrated evaluation for advanced removal of nitrate and phosphorus in novel PHBV/ZVI-based biofilters: Insight into functional genes and key enzymes. *J. Clean. Prod.* **2022**, *349*, 131199. [[CrossRef](#)]
39. Hao, W.; Zhang, J.; Duan, R.; Liang, P.; Huang, X. Organic carbon coupling with sulfur reducer boosts sulfur based denitrification by *Thiobacillus denitrificans*. *Sci. Total Environ.* **2020**, *748*, 142445. [[CrossRef](#)]
40. Morales-Gallardo, M.V.; Ayala, A.M.; Pal, M.; Cortes Jacome, M.A.; Toledo Antonio, J.A.; Mathews, N.R. Synthesis of pyrite FeS₂ nanorods by simple hydrothermal method and its photocatalytic activity. *Chem. Phys. Lett.* **2016**, *660*, 93–98. [[CrossRef](#)]
41. Amend, J.P.; Edwards, K.J.; Lyons, T.W. Sulfur Biogeochemistry—Past and Present. *Geol. Soc. Am. Spec. Pap.* **2004**, *379*, 195–205.
42. Chen, X.; Shi, T.; Zhong, K.; Wu, G.; Lu, Y. Capacitive behavior of MoS₂ decorated with FeS₂@carbon nanospheres. *Chem. Eng. J.* **2020**, *379*, 122240. [[CrossRef](#)]
43. Li, X.; Hu, Y.; Zhang, C.; Xiao, C.; Cheng, J.; Chen, Y. Electro-activating of peroxydisulfate via boron and sulfur co-doped macroporous carbon nanofibers cathode for high-efficient degradation of levofloxacin. *J. Hazard. Mater.* **2023**, *442*, 130016. [[CrossRef](#)] [[PubMed](#)]
44. Yamashita, T.; Hayes, P. Analysis of XPS spectra of Fe²⁺ and Fe³⁺ ions in oxide materials. *Appl. Surf. Sci.* **2008**, *254*, 2441–2449. [[CrossRef](#)]
45. Zhang, W.; Huang, F.Y.; Hu, W.W. Performance and mechanism of synchronous nitrate and phosphorus removal in constructed pyrite-based mixotrophic denitrification system from secondary effluent. *Environ. Sci. Pollut. Res.* **2020**, *27*, 36816–36825. [[CrossRef](#)] [[PubMed](#)]
46. Zhu, S. Mixotrophic Denitrification of Glucose Polymer-Based Pyrite Tailings for Enhanced Nitrogen and Phosphorus Removal of Municipal Tailwater. *Water* **2022**, *14*, 1868.

Disclaimer/Publisher’s Note: The statements, opinions and data contained in all publications are solely those of the individual author(s) and contributor(s) and not of MDPI and/or the editor(s). MDPI and/or the editor(s) disclaim responsibility for any injury to people or property resulting from any ideas, methods, instructions or products referred to in the content.